

RSC Advances



This is an *Accepted Manuscript*, which has been through the Royal Society of Chemistry peer review process and has been accepted for publication.

Accepted Manuscripts are published online shortly after acceptance, before technical editing, formatting and proof reading. Using this free service, authors can make their results available to the community, in citable form, before we publish the edited article. This *Accepted Manuscript* will be replaced by the edited, formatted and paginated article as soon as this is available.

You can find more information about *Accepted Manuscripts* in the [Information for Authors](#).

Please note that technical editing may introduce minor changes to the text and/or graphics, which may alter content. The journal's standard [Terms & Conditions](#) and the [Ethical guidelines](#) still apply. In no event shall the Royal Society of Chemistry be held responsible for any errors or omissions in this *Accepted Manuscript* or any consequences arising from the use of any information it contains.

Enhanced Catalytic and Antibacterial Activities of Silver Nanoparticles Immobilized on Poly(*N*-vinyl pyrrolidone)-Grafted Graphene Oxide

Shikha Singh,^a Ravi Kumar Gundampati,^b Kheyath Mitra,^a K. Ramesh,^{a,c} Medicherla V. Jaganaddam,^b Nira Misra,^c Biswajit Ray^{*a}

^aDepartment of Chemistry, Faculty of Science, Banaras Hindu University, Varanasi – 221005, India

^bMolecular Biology Unit, Institute of Medical Science, Banaras Hindu University, Varanasi – 221005, India

^cSchool of Biomedical Engineering, Indian Institute of Technology (Banaras Hindu University), Varanasi-221005, India

*Corresponding author. Email: biswajitray2003@yahoo.co.in

Abstract

Poly(*N*-vinyl pyrrolidone) (PNVP)-*grafted* graphene oxide (GO) (GO-PNVP) has been synthesized using a GO-based macro-RAFT agent prepared via click reaction of alkyne-terminated RAFT agent (S)-2-(Propynyl propionate)-(O-ethyl xanthate) and azide-functionalized GO (GO-N₃). FTIR, XPS, Raman, TGA and DSC studies confirmed its formation. Silver nanoparticles are then immobilized on GO-PNVP and GO *via in situ* reduction of silver nitrate in the presence and absence of glucose at 40 and 95 °C, respectively. FT-IR, UV-Vis, XRD, SEM and TGA studies supported the incorporation of silver (Ag) nanoparticles. Ag nanoparticles immobilized on GO-PNVP are small, spherical and narrowly distributed (homogenous, monodisperse) compared to GO. These nanocomposites are explored as catalysts for the reduction of *p*-nitrophenol into *p*-aminophenol and also as the antibacterial agents towards Gram(+) *S. aureus* and Gram(-) *E. coli* bacteria. Ag nanoparticles immobilized GO-PNVP showed efficient catalytic activity and excellent reusability along with an excellent antibacterial activity. Hence, grafting of PNVP enhances the catalytic and antibacterial properties of GO.

Introduction

Several reports have recently been focused on the immobilization of nanoparticles onto suitable substrates in order to prevent their agglomeration or, to enhance their efficiency through a proper interaction with the substrate. Such approach shows a promising application in optical, electronics, optoelectronic, electrochemical nanodevices and catalysis etc. Recently, silica,¹ alumina,² zeolites³, different types of carbon materials⁴ etc are used as substrate to immobilize nanoparticles. Morphology of nanomaterials, which varied from substrate to substrate, is an important factor to influence their properties. Graphene and its derivatives are excellent substrates for catalysis as these materials possess large surface area, unique thermal and chemical stability, excellent mechanical strength, and electrical conductivity.⁵⁻⁷ Out of these, graphene oxide (GO) has the reduction capability for metal precursors even at 0 °C,⁸ but, GO itself simultaneously reduces to partially reduced graphene (RG) which undergoes agglomeration; such agglomeration hampers or, obstructs the formation and growth of nanoparticles.

Water soluble and biocompatible polymer poly(*N*-vinyl pyrrolidone) (PNVP), used widely in pharmaceutical, cosmetic industries etc., can regulate the size and shape of nanoparticles during synthesis by exhibiting dual characters of reducing as well as stabilizing agent (protecting agent).⁹ Guo et al.¹⁰ and Nandi et al.¹¹ synthesized recently PNVP grafted covalently on GO and used the same as humidity sensors and compatibilizer. Herein, we report the synthesis of PNVP-grafted GO as substrate material to immobilise the nanoparticles in anticipation that it can regulate the size of nanoparticles together with the enhancement of the dispersibility of GO in polar solvents.

Out of all reported metal nanoparticles, silver nanoparticles received huge attention because of highest electrical conductivity,¹² antibacterial properties¹³⁻¹⁵ and excellent

catalytic properties.¹⁶ Therefore, the synthesis and immobilization of silver nanoparticles on a suitable substrate have been largely focussed by a considerable number of researchers.¹⁷⁻²² Silver nanoparticles, from a catalytic perspectives, are unique material for a number of important processes in the chemical industries for e.g., the selective oxidation of alkenes and alkanes²³⁻²⁴ and the reduction of 4-nitrophenols (4-NP) to 4-aminophenols (4-AP) which is a potent intermediate in the manufacturing of many analgesic and antipyretic drugs and nonhazardous materials such as paracetamol, phenacetin etc.²⁵⁻²⁶

Here, we report the synthesis of PNVP-grafted GO (GO-PNVP) via click chemistry and reversible addition-fragmentation chain transfer (RAFT) polymerization methods and used the same as a substrate material for the *in-situ* immobilization of Ag nanoparticles in the presence or, absence of glucose as reducing agent. First, graphene oxide (GO) is synthesized using improved Hummers method.²⁷ Then, its –OH functional group is converted into the corresponding bromo-derivative (GO-Br) on reaction with 2-bromopropionyl bromide. This GO-Br is converted into its corresponding azide-derivative (GO-N₃) on reaction with sodium azide. GO-N₃ is then reacted with alkyne terminated RAFT agent (S)-2-(Propynyl propionate)-(O-ethyl xanthate) via click chemistry to prepare xanthate RAFT agent-functionalized GO (GO-X). This GO-X is used as macro-RAFT agent for the synthesis of PNVP-grafted GO (GO-PNVP) via the RAFT polymerization of NVP using AIBN as initiator in DMF at 60 °C. Thereafter, Ag nanoparticles are immobilized on GO and GO-PNVP substrates *via* the *in-situ* reduction of silver nitrate in the presence and absence of glucose at 40 and 95 °C, respectively. Finally, we investigated the catalytic efficiency of these Ag nanoparticles-immobilized GO/GO-PNVP substrates for the conversion of 4-NP to 4-AP in the presence of sodium borohydride reducing agent. Moreover, antibacterial activities of these are also investigated by determining growth rate and minimal inhibitory concentration of a Gram-negative bacterium *E. coli* and a Gram-positive bacterium *S. aureus*. In addition,

an enzymatic assay study is performed using *E. coli* as representative bacterial model for the understanding of anti-bacterial activity.

Experimental section

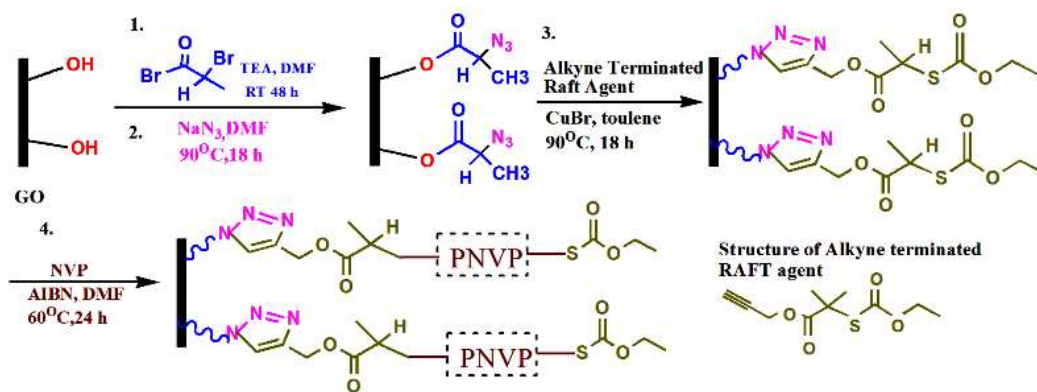
Materials

α -Bromopropionyl bromide (98%, Aldrich, USA), triethylamine (TEA) (99%, S.d fine chemicals, India), sodium azide (99%, Loba Chemie, India), CuBr (98%, Aldrich, USA), anhydrous MgSO₄ (Loba Chemie, India), hexane (CDH, India), tetrahydrofuran (THF) (98%, Loba Chemie, India), carbon disulphide (CS₂) (95% Loba Chemie, India), propargyl alcohol (98%, Loba Chemie, India), glucose (Fisher Scientific, India), AgNO₃ (S.d.fine chemicals, India), diethyl ether (S.d.fine chemicals, India), NaHCO₃ (S.d.fine chemicals, India), 4-nitrophenol (4-NP) (S.d. fine chemicals, India) were used as received. Cuprous bromide (CuBr, 98%, Aldrich, Steinheim, Germany) was purified using a reported procedure and dried under vacuum.²⁸ *N*-vinylpyrrolidone (NVP, 99%, Aldrich, USA) was dried over anhydrous calcium hydride and distilled under reduced pressure. 2,2'-azobis(isobutyronitrile) (AIBN) (98%, Spectrochem, India) was recrystallized from methanol. Anhydrous dimethyl formamide (DMF) (99%, Spectrochem, India) used after two step distillations: azeotropic distillation with benzene followed by distillation over anhydrous MgSO₄. Dry ethanol (Saraya Distilliary, India) was prepared by leaving over CaO for overnight followed by distillation over fresh CaO. Deionised water was prepared by redistillation of the double distilled water in an all glass distillation apparatus. (S)-2-(Propynyl propionate)-(O-ethyl xanthate) (X3) was synthesized following the method reported by our group.²⁹ GO was prepared using the improved Hummers method.²⁷

Characterization

FT-IR spectra were recorded using a PERKIN ELMER Spectrum version 10.03.05. instrument spectrometer in the range of 400-4000 cm⁻¹. UV visible spectra were recorded on

SHIMADZU UV-1700 pharma spec. Raman spectra of GO and all nanocomposites were taken by RENISHAWRM 1000 Raman spectrophotometer having Argon-ion (Ag^+) laser source of 514.5 nm. Thermogravimetric analysis (TGA) was performed using PERKIN ELMER-STA 6000 thermogravimetric analyser in the temperature range from 30-600 °C with a heating rate of 20 °C/min under N_2 atmosphere. Differential scanning calorimeter (DSC) measurement was performed using METTLER STAR SW 10.00 DSC instrument under N_2 atmosphere at a heating rate of 20 °C/min. The instrument was calibrated with indium before use. The XPS measurement was made in a Ultra high vacuum AMICUS photoelectron spectrometer equipped with $\text{MgK}\alpha$ X-ray as a primary excitation and a KRATOS VISION 2 SOFTWARE. The curve fitting of high resolution spectra were performed with combined Gaussian-Lorentzian functions. The morphology of PNVP grafted GO was observed using Scanning Electron Microscope QUANTA 200F operated at an acceleration voltage of 20 KV. Average size of nanoparticles was reported as the average of the diameters of 50 numbers of particles observed in the SEM micrographs. The scattering pattern of the powder samples was recorded in a X-Ray diffractometer BRUKER ECO D8 ADVANCE. Samples were grinded well before measurement, and the diffractogram was recorded using nickel-filtered Cu tube, $\text{K}\alpha$ radiation with 2θ ranging from 5° to 80°. Zeta potentials were measured using HORIBA-Nanoparticles analyzer SZ-100, Japan at 25°C for reference samples dispersed in deionised water (0.1mg/mL) after ultrasonication for 15 min.

Scheme 1 Synthesis of poly(*N*-vinyl pyrrolidone)-grafted graphene oxide (GO-PNVP)

Preparation of bromo-functionalized graphene oxide (GO-Br)

GO (300 mg) (prepared using Improve Hummers method²⁷) taken in a 500 mL round bottom flask was vacuum dried for 2 h and purged with nitrogen. Anhydrous DMF (200 mL) were then added to the flask and sonicated for 1 h to prepare a colloidal suspension of graphene oxide. To it, TEA (6 mL, 0.04 mmol) was added. Then, α -bromopropionyl bromide (9 mL, 0.08 mmol) was added dropwise to the above reaction mixture under stirring at 0°C . The resulting mixture was stirred for 3 h at 0°C and then at room temperature 48 h under N_2 atmosphere. The solid was then separated from the final reaction mixture via filtration, washed with chloroform, excess of deionised water and finally with acetone and then dried under high vacuum for 24 h at room temperature.

Preparation of azide-functionalized graphene oxide (GO- N_3)

GO-Br (250 mg) dispersed in anhydrous DMF (150 mL) via sonication. To it, NaN_3 (231.5 mg, 3.56 mmol) were then added. The resulting mixture was stirred for 18 h at 70°C under N_2 atmosphere. The resultant mixture was then transferred to the deionised water with vigorous stirring. The final product (GO- N_3) was collected by centrifugation and washed repeatedly with excess of deionised water and finally washed with acetone and then dried under high vacuum for 24 h at room temperature.

Preparation of RAFT-agent functionalized graphene oxide (GO-X) by click reaction

GO-N₃ (200 mg) were added into the dry DMF (60 mL) and dispersed by sonication. To it, CuBr (1.907 mg, 0.01 mmol) and DMF solution of alkyne-terminated raft agent X3 (79.344 mg, 0.342 mmol) were added. The resultant mixture was transferred to an oil bath maintained at 90 °C and stirred for 18 h. For workup, the resultant product was obtained by centrifugation and washed with excess of DMF to remove unreacted alkyne-terminated RAFT agent followed by washing with excess of methanol and water, finally with acetone. The obtained black solid product (GO-xanthate, GO-X) was dried under high vacuum for 24 h at 40 °C.

Preparation of poly(*N*-vinyl pyrrolidone)-grafted graphene oxide (GO-PNVP) by RAFT polymerisation

GO-X (150 mg) was dispersed in dry DMF (50 mL) by sonication. To it, AIBN (5.615 mg, 0.0342 mmol) and NVP (1.8 mL, 17.1 mmol) were added. The resultant mixture was transferred to an oil bath maintained at 60 °C and kept at this temperature under stirring for 24 h. Resultant reaction mixture was dried under vacuum and dissolved in 2 mL THF and precipitated from 300 mL hexane. This process of dissolution in THF and precipitation from hexane was repeated twice. The final product was separated by centrifugation and dried under vacuum at 40 °C for 24 h.

***In situ* synthesis of GO-supported silver nanoparticles in the absence of glucose (GO-Ag 95)**

GO (25 mg) was dispersed in 50 mL of water under sonication for 1 h. AgNO₃ (18.75 mg, 0.17 mmol, 75 wt % with respect to GO) was added to the above GO suspension. The dispersion containing GO and AgNO₃ was stirred at room temperature for 60 min to ensure

the homogenous mixing and then transferred to an oil bath maintained at 95 °C for 20 h. The obtained product was filtered and freeze-dried.

***In situ* synthesis of GO-PNVP supported silver nanoparticles in the absence of glucose (GO-PNVP-Ag 95)**

GO-PNVP (15 mg) was dispersed in 25 mL of water under sonication for 10 min. AgNO₃ (75 wt % with respect to GO, 11.25 mg, 0.10 mmol) was added to the above GO-PNVP suspension. The dispersion containing GO-PNVP and AgNO₃ was stirred at room temperature 60 min for homogenous mixing and transferred to an oil bath maintained at 95 °C for 20 h. The obtained product was filtered and freeze-dried.

***In situ* synthesis of GO-supported silver nanoparticles in the presence of glucose (GO-Ag 40)**

GO (25 mg) was dispersed in 50 mL of water under sonication for 1 h. AgNO₃ (75 wt% with respect to GO, 18.75 mg, 0.17 mmol) was added to the above GO suspension. After the complete dissolution of AgNO₃, glucose (33.75mg, 0.18 mmol) was added to above suspension and then kept under stirring at 40 °C for 20 h. The obtained product was filtered and freeze-dried.

***In situ* synthesis of GO-PNVP-supported silver nanoparticles in the presence of glucose (GO-PNVP-Ag 40)**

GO-PNVP (15 mg) was dispersed in 25 mL of water under sonication for 10 min. AgNO₃ (75 wt% with respect to GO-PNVP, 11.25 mg, 0.10 mmol) was added to the above GO suspension. After the complete dissolution of AgNO₃, glucose (20.25mg, 0.10 mmol) was

added to above suspension and then kept under stirring at 40 °C for 20 h. The obtained product was filtered and freeze-dried.

Catalytic studies

To a vial containing 3 mL of freshly prepared 10 mM NaBH₄ solution, 25 μL (10 mM) of 4-NP solution was added. This was followed by the addition of a specific amount of immobilized Ag nanoparticles (best studied at 0.5 mg catalyst). The solution was thoroughly mixed, followed by measurements of time-dependent absorption at 400 nm. Each individual catalytic study using nanocomposites was performed in quadruplicate.

Antibacterial studies

Growth curves of bacterial cells exposed to nanocomposites

To determine the growth curves of Gram-positive *Staphylococcus aureus* (*S. aureus*) and Gram-negative *Escherichia coli* (*E. coli*) cells exposed to nanocomposite samples (at 5 μg/mL concentration). The bacterial cell concentration was adjusted to 4×10^6 CFU/mL and incubated in a shaking incubator up to 6 h at 37 °C. Growth curves of bacterial cell cultures were attained through measures of the optical density at 600 nm. All measurements were carried out in triplicate.

Determination of minimum inhibitory concentration

The anti-bacterial activity of normal GO-PNVP, GO-Ag 40 and GO-PNVP-Ag 95 were determined by using LB (Luria–Bertani; LB) broth as diluent for the bacterial strains. Inoculates were prepared by suspending the overnight culture growth in sterile LB media. The prepared samples were dispensed into 10 mL of a sterile 0.8 wt% saline water containing about 10^6 cfu/mL of *E. coli* and *S. aureus*, and then shaken at 37 °C. Two-fold dilution of reference sample and standard drug sample in the 96-well plates were prepared. The final

volume in each well plate was 0.2 mL and was incubated at 37 °C for 24 h. The microwell plates were read at 590 nm using an ELISA reader to determine the MIC value. MIC was defined as the lowest concentration of an anti-microbial studied compound that inhibits the visible growth of a microorganism after overnight incubation.³⁰

Evaluation of anti-bacterial mechanism

The anti-bacterial effect of GO nanocomposites was determined by measuring the activity of β -D-galactosidase. A modified *o*-nitrophenol- β -D-galactopyranoside (ONPG) test procedure was used in this experiment.³¹⁻³² Standard solution containing a cell suspension of 1 mL with a concentration of 10^6 CFU mL⁻¹ and 1 mL of ONPG solution with a concentration of 25 mM were added simultaneously into 5.5 mL PBS buffer solutions (pH 7.4) and kept at 37 °C incubator for 15 min under shaking. Then, four different types of GO each of 100 μ L (0.5 μ g mL⁻¹) were added into a 96-well plate and labelled separately. Then 100 μ L of the above standard solutions containing the cell suspensions and ONPG in PBS buffer were added in the respective wells and labelled. At different time interval the changes of optical density at 420 nm (OD 420 nm) were measured by using a Multi-label Microplate Reader (Perkin Elmer VICTOR 3). At the same time two control samples such as bacterial strain with ONPG and PNVP (0.5 μ g mL⁻¹) with bacterial strain and PNVP were also measured.

Results and discussion

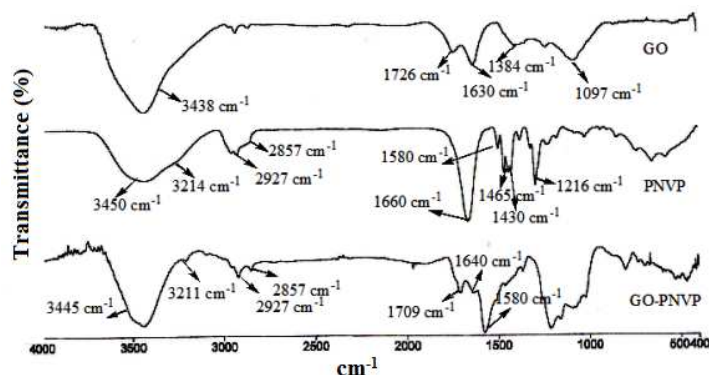


Fig. 1 FTIR spectra of GO, PNVP and GO-PNVP

FT-IR spectra of GO, PNVP and GO-PNVP are shown in **Fig. 1**. Spectrum of GO shows the strongest band at 3438 cm^{-1} corresponding to the O-H stretching vibrations (present in carboxylic acid and phenolic functional groups) associated through hydrogen bonding. Moreover, the presence of peaks at 1097 and 1384 cm^{-1} corresponding to C-O vibration and two other peaks at 1630 and 1726 cm^{-1} corresponding to the asymmetric and symmetric stretching COO vibrations of the carboxyl groups also support its formation. Apart from the characteristic peaks of GO, the spectrum of GO-PNVP shows the characteristic peaks of PNVP and aromatic triazole ring: OH stretching of hydrogen bonded water at 3450 cm^{-1} , carbonyl stretching (heteroatom present in the ring of pyrrolidone) at 3214 cm^{-1} , intense symmetric CH_2 stretching of the backbone chain of PNVP at 2927 cm^{-1} , C-H stretching at 2857 cm^{-1} , C=O stretching at 1709 cm^{-1} , amide and C-N stretchings at 1640 cm^{-1} , C=C aromatic ring vibration at 1580 cm^{-1} , CH_2 scissorings at 1465 cm^{-1} and 1430 cm^{-1} , CH bending at 1365 cm^{-1} , CH_2 twisting at 1216 cm^{-1} , C-C pyrrolidone ring breathing at 1017 cm^{-1} , C-C of the backbone chain at 810 cm^{-1} , and N-C=O bendings of the pyrrolidone ring at 671 and 597 cm^{-1} . All these characteristic peaks of PNVP confirmed the successful functionalization of GO with PNVP.³³

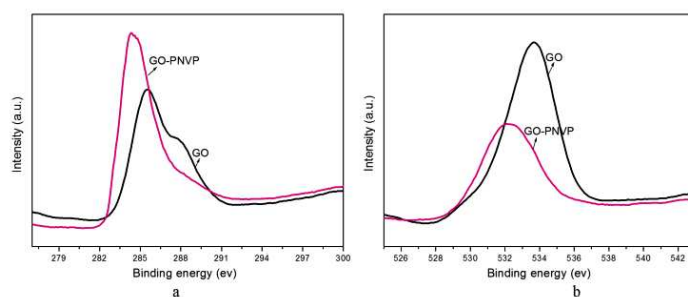


Fig. 2 XPS spectra of (a) C(1s) and (b) O(1s) region of GO and GO-PNVP.

XPS spectra of C (1s) and O (1s) region of GO and GO-PNVP are shown in **Fig. 2(a)** and **(b)**, respectively. The C (1s) signals of GO-PNVP is stronger than that of GO with a shifting in its binding energy to lower side (284.1 eV) corresponding to the aliphatic hydrocarbon (C-C, C-H) of PNVP backbone chain. But the O (1s) signal of GO-PNVP is weaker with respect to that of GO. The C/O area ratio is increased in GO-PNVP owing to the increase in the carbon skeleton. These observations reveal the successful functionalization of PNVP on the GO.

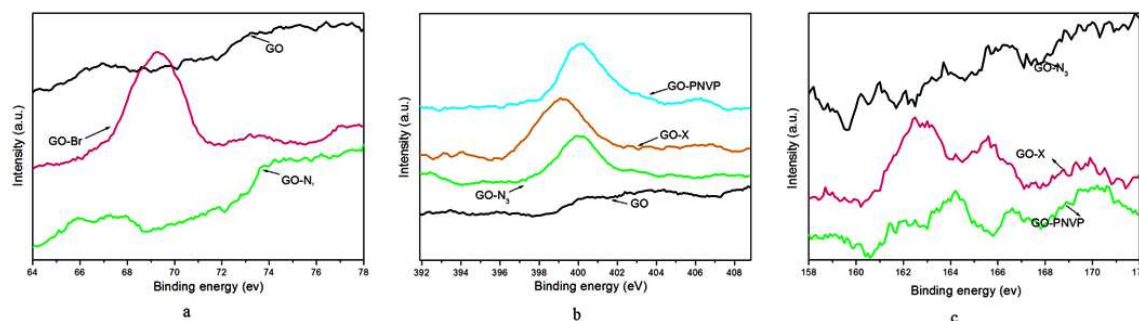


Fig. 3 XPS spectra of (a) Br(3d) region of GO, GO-Br and GO-N₃ (b) N (1s) region of GO, GO-N₃, GO-X and GO-PNVP (c) S (2p) region of GO-N₃, GO-X and GO-PNVP.

XPS spectra of Br (3d) region GO, GO-Br and GO-PNVP are shown in **Fig. 3 (a)** Br-terminated precursor GO-Br exhibits a strong peak at 70 eV which are assigned to Br (3d) signal. Absence of this peak in GO and GO-N₃ indicates the successful bromination of GO with α -bromopropionyl bromide and replacement of bromine by azide. XPS spectra of N (1s) region of GO, GO-N₃, GO-X and GO-PNVP are shown in **Fig. 3 (b)** In case of GO-

PNVP, the observed shifting to the higher binding energy side (401 eV) corresponds to $-N-C=O$ group of PNVP.³⁴ XPS spectra of S (2p) region of GO-N₃, GO-X and GO-PNVP are shown in **Fig. 3 (c)** Sulphur terminated precursor GO-X revealed a strong peak at 162.5 eV. This peak is absent in case of GO-N₃. Thus, it reveals the presence of xanthate in the sample. Curve fitting of XPS spectra are shown in **Fig. S2 (Supporting Informations)**. Other characterizations such as Raman, XRD, TGA and DSC also support its formation (**Fig. S1, S3 and S4, Supporting Informations**). All these results indicate the successful PNVP functionalization of GO.

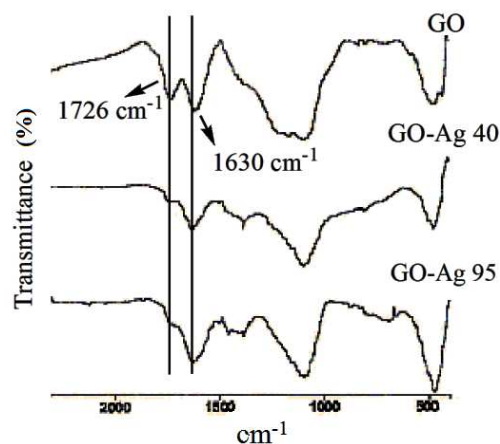


Fig. 4 FT-IR spectra of GO, GO-Ag 40 and GO-Ag 95.

The FT-IR spectra of GO, GO-Ag 40 and GO-Ag 95 are shown in **Fig. 4** After the incorporation silver nanoparticles, the peaks position of the functional groups on GO still remained unchanged but the peak associated with asymmetric (1726 cm^{-1}) COO vibration shown decrease in intensity whereas that of the symmetric (1630 cm^{-1}) COO vibration increased. Such change in peak intensity may be because of the interaction between the Ag nanoparticles and the oxygen containing functional group. This result was consistent with previous report.³⁵

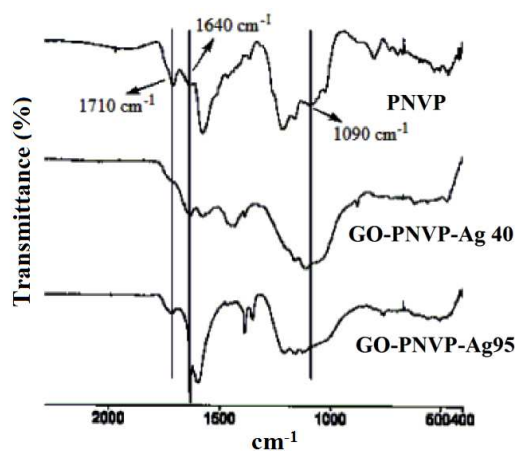


Fig. 5 FT-IR spectra of GO-PNVP, GO-PNVP-Ag 40 and GO-PNVP-Ag 95.

The FT-IR spectra of GO-PNVP, GO-PNVP-Ag 40 and GO-PNVP-Ag 95 are shown in **Fig. 5**. The peak associated with C=O stretching at 1710 cm^{-1} shows decrease in intensity while that of resonance peak of C=O, C-N stretching band at 1640 cm^{-1} shows increase or strengthened with no considerable change in peak position. Interestingly, the peak associated with C-N bending mode at 1090 cm^{-1} in GO-PNVP shifts to high wave number in GO-PNVP-supported silver nanoparticles samples. This may be due to the interaction of the lone pair of nitrogen with Ag. Thus, Ag nanoparticles are preferentially stabilized via coordination through the lone pair of nitrogen.³⁶

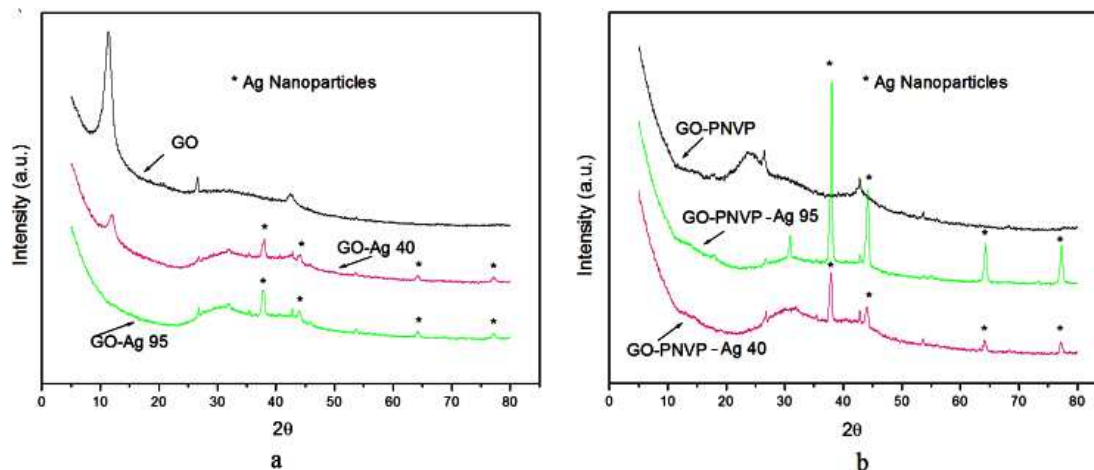


Fig. 6 XRD spectra of (a) GO, GO-Ag 40 and GO-Ag 95 and (b) GO-PNVP, GO-PNVP-Ag 40 and GO-PNVP-Ag 95

To confirm the inclusion of Ag nanoparticles in GO-Ag 40, GO-Ag 95, GO-PNVP-Ag 40 and GO-PNVP-Ag 95 samples, XRD spectra was carried out (**Fig. 6**). The XRD spectra of these samples show the characteristic diffraction peak of Ag at 2θ values of about 38.1 , 44.3 , 64.5 and 77.5° corresponding to (111), (200), (200) and (311) crystallographic planes of face centred cubic (fcc) lattice of metallic silver nanoparticles (JCPDS No. 04-0783). In case of GO-PNVP-Ag systems, the presence of a new sharp peak at 2θ values of about 30.8° is also observed. Similar observation is also reported in the literature.³⁷ Presently, it is not clear to us. Therefore, XRD study confirms the incorporation of Ag nanoparticles in GO/GO-PNVP substrates.

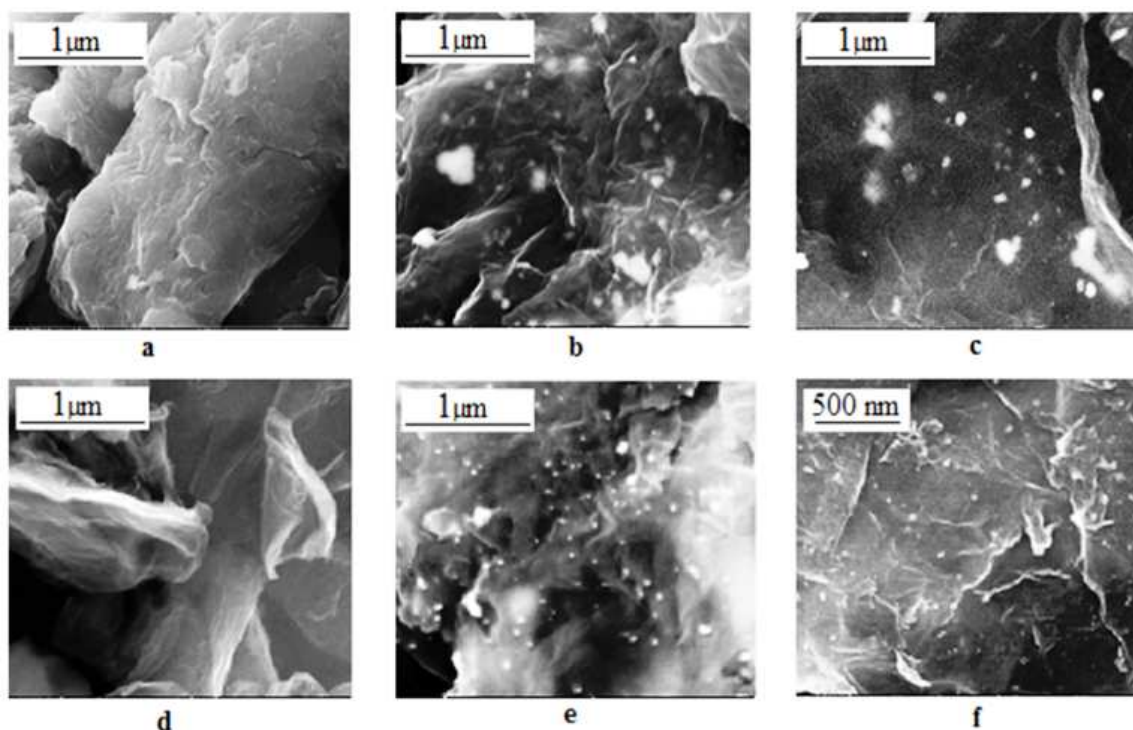


Fig. 7 SEM images of (a) GO (b) GO-Ag 40 (c) GO-Ag 95 (d) GO-PNVP (e) GO-PNVP-Ag 40 and (f) GO-PNVP-Ag 95.

To get the idea about the size and shape of Ag nanoparticles in GO/GO-PNVP substrates SEM technique is used. **Fig. 7** shows the scanning electron micrographs of the GO, GO-Ag 40, GO-Ag 95, GO-PNVP, GO-PNVP-Ag 40 and GO-PNVP-Ag 95 samples. GO and PNVP samples show clearly the absence of nanoparticles, whereas all the other systems have Ag nanoparticles. The average size of Ag nanoparticles in GO-Ag 40, GO-Ag 95, GO-PNVP-Ag 40 and GO-PNVP-Ag 95 systems are 58, 102, 30 and 15 nm, respectively. The Ag nanoparticles over GO-PNVP substrate are small, spherical and narrowly distributed (homogenous, monodisperse), whereas, in case of GO as substrate, it shows the formation of non-homogeneous and relatively larger nanoparticles. This result implies that the presence of the grafted PNVP on GO plays an important role as stabilizer on the nucleation and growth of silver nanoparticles.

UV-Vis spectra and TGA thermograms of GO-Ag and GO-PNVP Ag systems also support the incorporation of Ag nanoparticles in GO / GO-PNVP (**Fig. S5 and S7, Supporting Informations**)

Catalytic studies

4-aminophenol (4-AP) is a well known organic compound, useful in many applications, including analgesic and antipyretic drugs,²⁵⁻²⁶ photographic developers,³⁸ corrosion inhibitors³⁹ and anticorrosion lubricants.⁴⁰ So, the reduction of *p*-nitrophenol (4-NP) by NaBH₄ in the presence of noble metal nanoparticles catalysts has been intensively investigated.¹⁷⁻²² Here, we monitored the time dependent extent of the conversion of 4-NP to 4-AP using prepared four different catalysts: GO-Ag 40, GO-Ag 95, GO-PNVP-Ag 40, and GO-PNVP-Ag 95. Under neutral or, acidic conditions, aqueous 4-NP solution exhibits a strong absorption peak at 317 nm.¹⁷ Upon the addition of NaBH₄, the alkalinity of the solution increases and the absorption peak shifts to 400 nm. When GO is added into the aqueous mixture of 4-NP and NaBH₄, the peak remains unaltered with time. However, the addition of a small amount of prepared catalysts (Ag-nanoparticles immobilized substrates) causes the rapid fading and ultimate bleaching of the yellow colour (absorption peak at 400 nm) with the appearance of the new peaks at 230 nm and 298 nm corresponding to 4-AP. These changes indicate the successful conversion of 4-NP to 4-AP. The whole reduction process of each substrate was monitored by measuring the time dependant UV-vis absorption spectra of the reaction mixture solution (**Fig. S8, Supporting Informations**).

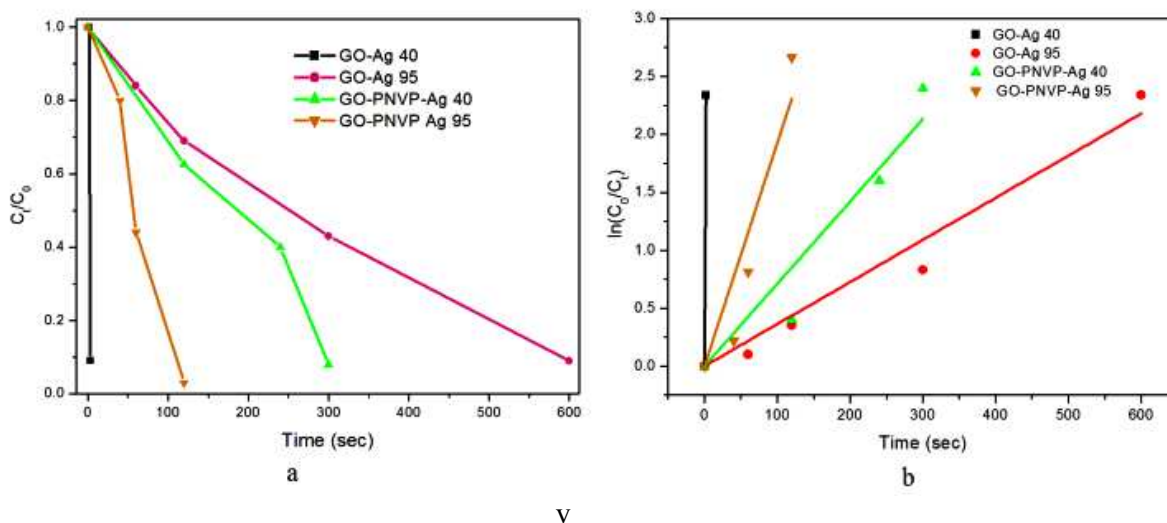


Fig. 8 Plots of (a) C_t/C_0 and (b) $\ln(C_0/C_t)$ (C_0 = absorbance of 4-NP at 400 nm at initial time, C_t = absorbance of 4-NP at 400 nm at specific time interval t) vs. reaction time at room temperature (27 °C)

Almost linear correlation is observed in the plot between $\ln(C_0/C_t)$ (C_0 = absorbance of 4-NP at 400 nm at initial time, C_t = absorbance of 4-NP at 400 nm at specific time interval t) and reaction time for all supported Ag catalyst systems at room temperature (27 °C) [Fig. 8]. So, the reduction reaction is pseudo first order type as expected. The pseudo first order rate constants (k) at 27 °C calculated from the corresponding slopes (fitted) are 1.17, 3.6×10^{-3} , 7.1×10^{-3} and $1.9 \times 10^{-2} \text{ s}^{-1}$ for GO-Ag 40, GO-Ag 95, GO-PNVP-Ag 40 and GO-PNVP-Ag 95 systems, respectively. The corresponding calculated TOFs (turn over frequency,⁸ the number of reactant molecules that 1 g of catalyst can convert into product in the given interval of time) are 1.50×10^{20} , 5.0×10^{17} , 1.0×10^{18} , and $2.51 \times 10^{18} \text{ molecules g}^{-1} \text{ s}^{-1}$, respectively. All the four catalysts exhibited different rates of reaction along with its efficiency. These results clearly indicate that the catalytic properties of Ag nanoparticles are influenced by the size of the nanoparticles and the nature of the substrate materials used for immobilization. Out of all these supported catalysts, GO-Ag 40 shows an excellent rate of

reaction with high TOF compared to others. Though particle size of this system is ~ 58 nm, but *in situ* synthesis of Ag- nanoparticles involving glucose as reducing agent led to partial reduction of GO also, making it less defective and more aromatic like RG (reduced graphene) type.²² Thus, the base substrate become more compatible with aromatic 4-NP and adsorbed it easily through π - π stacking, making the reduction process much more facile for immobilized Ag nanoparticles.^{8,41} Whereas for GO-PNVP-Ag 95 and GO-PNVP-Ag 40 systems, the immobilizing surface of GO-PNVP is like GO (more defective and less aromatic) and populated with grafted PNVP chains, which made it much less compatible with 4-NP as π - π stacking is very much hindered. So, here, GO-PNVP-Ag 95 having smaller size (~ 15 nm) and well distributed Ag nanoparticles with effectively larger surface area showed faster reaction rate as compared to GO-PNVP-Ag 40 system having distributed nanoparticles of larger sized (~ 30 nm). GO-Ag 95 system is the least reactive amongst the four. Here, GO itself acted as reducing agent for Ag nanoparticle generation.⁸ The corresponding nanoparticles are of much larger size (~ 102 nm) having much less surface to volume ratio and much less abundant. Moreover, the base substrate remained more defective, less aromatic and less compatible with 4-NP.

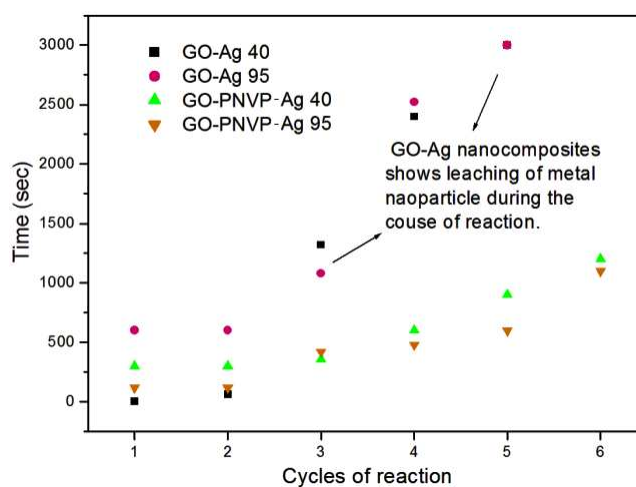


Fig. 9 Recyclability of catalysts (GO-Ag 40, GO-Ag 95, GO-PNVP-Ag 40, GO-PNVP-Ag 95) for the conversion of 4-nitro-phenol into 4-amino-phenol.

We further investigated the recyclability of these catalysts (GO-Ag 40, GO-Ag 95, GO-PNVP-Ag 40, and GO-PNVP-Ag 95). For this, we carried out a set of reactions, in sequence, where the ratio of the amount of catalyst and the reactants were kept the same. Once the reaction was completed (as observed by the disappearance of the characteristic absorption peak of 4-NP at 400 nm), the catalysts were recovered by decantation of the product reaction mixture. This was followed by washing of the solid composite with deionised water. Then, 3 mL of the same starting reaction mixture was added to the cuvette containing the washed catalyst. The absorbance decay of 4-NP with time was monitored as before. The completion of the reaction was taken as the second cycle. Similarly, the total number of cycles repeated was six using the same catalyst. The results for all catalysts are shown in **Fig. 9**. It reveals that the catalytic activity is retained quite well in GO-PNVP-Ag system compared to GO-Ag system. For example, in case of GO-Ag-40, the reaction was completed in 2 s in the first cycle; but it took 3000 s to be completed in the fifth cycle. The same reaction in case of GO-PNVP-Ag-40 took only 900 s in the fifth cycle. The apparent difference between the successive cycles could be due to the loss of catalyst during washing in between two cycles. The nanoparticles adhered to the surface of GO-PNVP have greater affinity via the pyrrolidone group of PNVP system as compared to GO (which partially reduced during the Ag nanoparticles synthesis) and prevent the leaching of Ag nanoparticles during the course of reaction. From systematic survey of literature for the catalytic conversion of 4-NP into 4-AP using NaBH_4 as reducing agent, Ag-nanoparticle loaded GO-PNVP emerges as an efficient, workable, easily recoverable and reusable Ag nanoparticle catalyst with reasonably high TOF [**Table S9** (*Supporting information*)]. Such supported Ag catalyst will eventually be useful in lowering the production cost in industry.

Antibacterial studies

The antibacterial activities of PNVP, GO-PNVP, GO-Ag-40 and GO-PNVP-Ag-95 were also investigated by determining growth rate and minimal inhibitory concentration of a Gram-negative bacterium *E. coli* and a Gram-positive bacterium *S. aureus*. To measure the growth rate of bacteria, cells were cultured in LB broth with PNVP, GO-PNVP, GO-Ag-40 and GO-PNVP-Ag-95 and the growth was monitored by the measurement of increase in optical density (OD) at 600 nm. The obtained reliable growth curves of *E. coli* and *S. aureus* are shown in **Fig. 10(a)** and **(b)**. Except PNVP all the other samples exhibit antibacterial

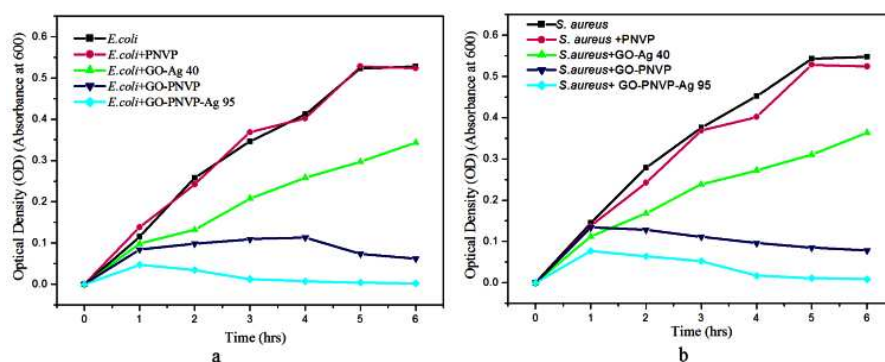


Fig. 10 Effect of PNVP, GO-PNVP, GO-Ag 40 and GO-PNVP-Ag 95 at 5 $\mu\text{g}/\text{mL}$ on the growth of **(a)** *E. coli* and **(b)** *S. aureus* at 10^6 CFU/mL concentration.

activities for both Gram-positive and Gram-negative bacteria. Using 5 $\mu\text{g}/\text{mL}$ concentration, GO-PNVP-Ag 95 completely inhibited the bacteria cell growth of both Gram-negative *E. coli* and Gram-positive *S. aureus* after around 4 h. So, among all the samples studied, GO-PNVP-Ag-95 showed excellent antibacterial property. In order to obtain more comprehensive antibacterial activities of these nanocomposites and their lowest concentrations which completely inhibit bacterial cell growth, we measured the minimal inhibitory concentration (MIC) of these nanocomposites against both bacteria species as shown in **Table 1**. The result clearly indicates that the MIC values of Gram-negative bacteria are lower

Table 1. Summary of minimal inhibitory concentration ($\mu\text{g/mL}$) against Gram-negative and Gram-positive bacteria

Bacterial strain	GO-Ag 40	GO-PNVP	GO-PNVP-Ag 95
<i>E.coli</i> (Gram-)	0.56	0.23	0.17
<i>S. aureus</i> (Gram +)	2.3	2.26	1.92

than those of Gram-positive bacteria. The observed trend may be from the distinct structure of cell wall between Gram-negative and Gram-positive bacteria. The cell wall of Gram-negative bacteria *E. coli* is composed of thin peptidoglycan (mesh-like polymer consisting of sugars and amino acids) layer (7-8 nm) with an additional outer membrane; whereas, Gram-positive bacteria *S. aureus* contains a thick peptidoglycan layer (20-80 nm) at the outside of the cell wall without any additional outer membrane. The thick peptidoglycan of Gram-positive bacteria may also include other components such as teichoic and lipoteichoic acids and complex polysaccharides, which serve to act as chelating agents and protects against antibacterial agents such as antibiotics, toxins, chemical, and degradative enzymes. Moreover, the antibacterial activity of Ag-nanoparticles incorporated in GO-PNVP substrates is superior with respect the other related reports of graphene oxide and its derivatives over *E. coli* and *S. aureus* as shown in **Table-S10** (*Supporting Informations*).

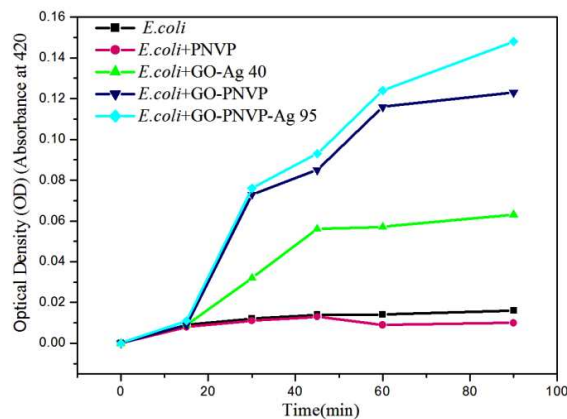


Fig. 11 Optical density (OD) curves indicating the absorption of *o*-nitrophenol (ONP) from different well plates at different time periods

To understand the anti-bacterial effect of these nanocomposites in more details, a β -D-galactosidase-based enzymatic assay has been performed using *E. coli* as representative bacterial model. β -D-galactosidase is an exoglycosidase (hydrolase enzyme) which presents both in the human body and microorganisms such as *E. coli* and exhibits hydrolyzing activity for the β -D-glycosidic bond present in sugar (disaccharides), fat and glycosides. By the action of antibacterial agent, β -D-galactosidase will leak out from the dead bacteria cells (*E. coli*), and eventually catalyze the hydrolysis of *o*-nitrophenol- β -D-galactopyranoside (ONPG) in the medium into *o*-nitrophenol (ONP) which has the specific absorption at 420 nm. Samples were added into the cell suspension containing ONPG and the absorption at 420 nm was measured at different time intervals. The optical density (OD) curves are shown in **Fig. 11**. OD of the untreated *E. coli* in the control well without any anti-microbial agent remained intact as there was no release of β -D-galactosidase into the suspension to catalyze ONPG. *E. coli* treated with PNVP also exhibited no significant absorbance changes at the measured time period. This result indicates that the catalytic effect or, interaction of PNVP does not promote the conversion of ONPG into ONP i.e., antibacterial activity. However, GO-PNVP, GO-Ag 40 and GO-PNVP-Ag 95 nanocomposites significantly disrupt the cell membrane of *E. coli* as absorption at 420 nm increases with time. Ag nanoparticles⁴² as well as GO^{43,44} are

reportedly efficient antibacterial agents. Generally, Ag nanoparticles show antibacterial properties by inhibiting the respiratory chain of bacterial cell and via sustained release of Ag^+ inside the bacterial cell (environment of lower pH). These Ag^+ ions stimulates the production of reactive oxygen species (ROS) which eventually (i) destroy the bacterial cell, (ii) inactivate the bacteria protein, and (iii) inhibit the bacteria DNA replication, and electron transport.⁴² Whereas, GO sheets intertwine the pathogens and most likely block the cell membranes by mechanical wrapping resulting local perturbation and damage. This leads to disturbance in normal metabolism of cells by blocking water channels and the absorption of nutrients along with ROS production like Ag nanoparticles. All these eventually lead to the bacterial cell death.^{43,44} Any system containing both GO and Ag nanoparticles should expectedly show better antibacterial properties. Here, we have considered two composite systems, GO-Ag 40 and GO-PNVP-Ag 95, which showed excellent catalytic properties. Moreover, we have chosen GO-PNVP system to study the effect of the grafting of PNVP on GO. Among these three GO based systems, antibacterial activity of GO-Ag 40, although it contains Ag nanoparticles, is inferior to that of GO-PNVP and GO-PNVP-Ag 95. This may be because of the superior cell-adhesion properties of PNVP-grafted GO compared to GO owing to the higher complexing ability of the grafted PNVP with the functional groups of cell membrane and the higher dispersibility of the PNVP-grafted GO in the medium. Indeed, zeta potential study supports the higher dispersibility of GO-PNVP systems in deionized water (Table S11, and Figure S12, *Supporting informations*). GO-PNVP-Ag 95 shows relatively better antibacterial properties over GO-PNVP obviously owing to the presence of Ag nanoparticles. Therefore, grafting of PNVP on GO enhances its antibacterial properties.

Conclusion

PNVP-grafted GO has been synthesized using GO-based macro-RAFT agent prepared via click reaction of azide-functionalized GO and alkyne-terminated RAFT agent X3 and characterized by FTIR, Raman, XPS, TGA and DSC studies. Ag nanoparticles are then immobilized on the surface of GO and GO-PNVP. FT-IR, UV-Vis, Raman, XPS, TGA, DSC, and SEM studies support their formation. Variation of immobilizing substrate and reaction condition leads to considerable difference in the morphology and distribution of Ag nanoparticles. Nanoparticles immobilized on GO-PNVP substrate are small, narrowly distributed compared to that on GO. Using these nanocomposites, the catalytic effect for the reduction of *p*-nitrophenol to *p*-aminophenol, and the antibacterial properties towards Gram(+) *S. aureus* and Gram(-) *E. coli* bacteria are explored. GO-PNVP-Ag showed efficient catalytic activity and excellent reusability for the reduction process. This nanocomposite also showed an excellent antibacterial property compared to simple GO based composites. Hence, we conclude that *grafted* PNVP enhances the properties of GO as immobilizing base for Ag NP as the nanoparticles adhered to surface of GO-PNVP with greater affinity via the pyrrolidone group of PNVP and make it much suitable system for catalytic and antimicrobial application.

Acknowledgement

BR gratefully acknowledges the financial support of DST (Govt. of India) via DST Nano Mission Project. SS and KM acknowledge UGC (Govt. of India) and Banaras Hindu University for Research Fellowships. Authors acknowledge Prof. R. K Singh (Dept. of Physics, BHU), Prof. A. S. K Sinha (Dept. of Chemical Engineering, IIT-BHU) and Prof. P. Maiti (School of Material Science and Technology, IIT-BHU) for providing Raman, XPS and Zeta potential measurement facilities, respectively.

Notes and references

†Electronic Supporting Information (ESI) available

- 1 K. H. Park, S. U. Son and Y. K. Chung, *Org. Lett.*, 2002, **4**, 4361-4363.
- 2 H. Lim, J. Lee, S. Jin, J Kim, J. Yoon and T. Hyeon, *Chem. Commun.*, 2006, **4**, 463–465.
- 3 K. Cheng, J. Kang, S. Huang, Z. You, Q. Zhang, J. Ding, W. Hua, Y. Lou, W. Deng and Y. Wang, *ACS Catal.*, 2012, **2**, 441–449.
- 4 G. G. Wildgoose, C. E. Banks and R. G. Compton, *Small.*, 2006, **2**, 182 – 193
- 5 S. Sattayasamitsathit, Y. Gu, K. Kaufmann, W. Jia, X Xiao, M. Rodriguez, S. Minteer, J. Cha, D. B. Burckel, C. Wang, R. Polsk and J. Wang. *J. Mater. Chem. A.*, 2013, **1**, 1639–1645.
- 6 J. R. Potts, S. H. Lee, T. M. Alam, J. An, M. D. Stoller, R. D. Piner and R. S. Ruoff, *Carbon.*, 2011, **49**, 2615 –2623.
- 7 K. Zhang, L. L. Zhang, X. S. Zhao and J. Wu, *Chem. Mater.*, 2010, **22**, 1392–1401.
- 8 M-Q. Yang, X. Pan, N Zhang and Y-J Xu, *CrystEngComm.*, 2013, **15**, 6819–6828
- 9 H. S. Shin, H. J. Yang, S. B. Kim and L. M. Sang, *Journal of Colloid and Interface Science.* 2004, **274**, 89–94.
- 10 J. Zhang, G. Shen, W. Wang, X. Zhou and S. Guo, *J. Mater. Chem.*, 2010, **20**, 10824–10828.
- 11 R. K. Layek, A. Kuila, D. P. Chatterjee and A. K. Nandi, *J. Mater. Chem., A* 2013, **1**, 10863–10874.
- 12 A. H. Alshehri, M. Jakubowska, A. Młozniak, M. Horaczek, D. Rudka, C. Free and J. D. Carey, *ACS Appl. Mater., Interfaces.* 2012, **4**, 7007–7010.
- 13 A. R. Shahverdi, A. Fakhimi, H. R. Shahverdi and S. Minaian, *Nanomedicine: Nanotechnology, Biology, and Medicine* 2007, **3**, 168 – 171.

- 14 V. K. Sharma, R. A. Yngard and Y. Lin, *Advances in Colloid and Interface Science.*, 2009, **145**, 83–96.
- 15 Q. H. Tran, V. Q. Nguyen and A-T. Le, *Adv. Nat. Sci.: Nanosci. Nanotechnol.*, 2013, **4**, 033001-033020.
- 16 K. Shimizu, K. Sawabe and A. Satsuma, *Catal. Sci. Technol.*, 2011, **1**, 331–341.
- 17 A. Murugadoss and A. A. Chattopadhyay, *Nanotechnology.*, 2008, **19**, 015603-015611.
- 18 G-P. Yong, D. Tian, H-W. Tong and S-M. Liu, *Journal of Molecular Catalysis A. Chemical.*, 2010, **323**, 40–44.
- 19 W. Bai, F. N. J. Zheng and Q. Sheng, *ACS Appl. Mater. Interfaces.* 2014, **6**, 5439–5449.
- 20 S. Dutta, C. Ray, S. Sarkar, M. Pradhan, Y. Negishi and T. Pal, *ACS Appl. Mater. Interfaces.*, 2013, **5**, 8724–8732.
- 21 E. Martinsson, M. A. Otte, M. M. Shahjamali, B. Sepulveda and D. Aili, *J. Phys. Chem. C.*, 2014, **118**, 24680–24687.
- 22 X-Z. Tang, X. Li, Z. Cao, J. Yang, H. Wang, X. Pu and Z-Z. Yu, *Carbon.*, 2013, **59**, 93 – 99.
- 23 M. Akimoto, K Ichikawa and E. Echigoya, *J. Catal.*, 1982, **76**, 333–344.
- 24 M.A. Barteau and R. J. Madix, *J. Am. Chem. Soc.*, 1983, **105**, 344–349.
- 25 H. Li and J. J. Cooper-White. *Nanoscale.*, 2013, **5**, 2915.
- 26 M. J. Fernandez-Merino, L. Guardia, J. I. Paredes, S. Villar- Rodil, A. Martinez-Alonso and J. M. D. Tascon, *RSC Adv.*, 2013, **3**, 18323–1833.
- 27 D. C. Marcano, D. V. Kosynkin, J. M. Berlin, A, Sinitskii, Z. Sun, A. Slesarev, L. B. Alemany, W. Lu and J. M. Tour, *ACS Nano.* 2010, **4**, 4806–4814.

- 28 N. K. Vishwakarma, V. K. Patel, S. K. Hira, K. Ramesh, P. Srivastava, K. Mitra, Shikha. Singh, D. Chattopadhyay, P. Maiti, N. Misra, P. P. Manna and B. Ray, *RSC Adv.*, 2015, **5**, 15547-15558
- 29 V. K. Patel, N. K. Vishwakarma, A. K. Mishra, C. Biswas, P. Maiti and B. Ray, *J. Applied.. Polymer. Science.* 2013, **127**, 4305-4317.
- 30 J. M. Andrews, *J. Antimicrob. Chemoth.*, 2001, **48**, 5–16.
- 31 S. Chen, Y. Guo, S. Chen, H. Yu, Z. Ge, X. Zhang, P. Zhang and J. Tang, *J. Mater. Chem.*, 2012, **22**, 9092–9099.
- 32 B. Gao, S. He, J. Guo and R. Wang, *J. Appl. Polym. Sci.*, 2006, **100**, 1531–1537.
- 33 Y. Borodko, S. E. Habas, M. Koebel, P. Yang, H. Frei and G. A. Somorjai, *J. Phys. Chem. B.*, 2006, **110**, 23052-23059.
- 34 C. M. Santos, A. Kumar, W. Zhang and C. Cai. *Chem. Commun.*, 2009, **28**, 2854-2856.
- 35 K. S. Hui, K. N. Hui, D. A. Dinh, C. H. Tsang, Y. R. Cho, W. Zhou, X. Hong and H-H. Chun, *Acta Materialia.*, 2014, **64**, 326–332.
- 36 P. K. Sahoo, S. S. K. Kamal, T. J. Kumar, B. Sreedhar, A. K. Singh and S. K. Srivastava, *Defence Science Journal.*, 2009, **59**, 447-455.
- 37 S. U. D. Khan, B. Ahmed, S. K. Raghuvanshi and M. A. Wahab, *Indian Journal of Pure and Applied Physics.*, 2014, **52**, 192-197.
- 38 F. C. John, *Dyes and Pigments.*, 1999, **41**, 127-136.
- 39 C. V. Rode, M. J. Vaidya, and R. V. Chaudhari, *Organic Process Research & Development.*, 1999, **3**, 465-470.
- 40 S. Saha, A. Pal, S. Kundu, S. Basu and T. Pal, *Langmuir.*, 2010, **26**, 2885–2893
- 41 J. Li, C-Y. Liu and Y. Liu, *J. Mater. Chem.*, 2012, **22**, 8426–8430.
- 42 K. K. Y. Wong and X. Liu, *Med. Chem. Commun.*, 2010, **1**, 125-131.

43 J. Chen, H. Peng, X. Wang, F. Shao, Z. Yuan and H. Han, *Nanoscale.*, 2014, **6**, 1879–1889.

44 J. D. Mangadlao, C. M. Santos, M. J. L. Felipe, A. C. C. Leon de, D. F. Rodrigues and R. C. Advincola, *Chem. Commun.*, 2015, **51**, 2886—2889.